Interdecadal Change in Properties of El Niño–Southern Oscillation in an Intermediate Coupled Model

RONG-HUA ZHANG AND ANTONIO J. BUSALACCHI

Earth System Science Interdisciplinary Center (ESSIC), University of Maryland, College Park, College Park, Maryland

(Manuscript received 9 June 2004, in final form 30 September 2004)

ABSTRACT

The role of subsurface temperature variability in modulating El Niño–Southern Oscillation (ENSO) properties is examined using an intermediate coupled model (ICM), consisting of an intermediate dynamic ocean model and a sea surface temperature (SST) anomaly model. An empirical procedure is used to parameterize the temperature of subsurface water entrained into the mixed layer (T_e) from sea level (SL) anomalies via a singular value decomposition (SVD) analysis for use in simulating sea surface temperature anomalies (SSTAs). The ocean model is coupled to a statistical atmospheric model that estimates wind stress anomalies also from an SVD analysis. Using the empirical T_e models constructed from two subperiods, 1963–79 (T_e^{63-79}) and 1980–96 (T_e^{80-96}), the coupled system exhibits strikingly different properties of interannual variability (the oscillation period, spatial structure, and temporal evolution). For the T_e^{63-79} model, the system features a 2-yr oscillation and westward propagation of SSTAs on the equator, while for the T_e^{80-96} model, it is characterized by a 5-yr oscillation and eastward propagation. These changes in ENSO properties are consistent with the behavior shift of El Niño observed in the late 1970s. Heat budget analyses further demonstrate a controlling role played by the vertical advection of subsurface temperature anomalies in determining the ENSO properties.

1. Introduction

El Niño has been observed to exhibit interdecadal changes in its properties, including oscillation period and propagation characteristics of SSTAs (e.g., Trenberth and Hurrel 1994; Miller et al. 1994; An and Wang 2000). For example, the dominant oscillation periods of El Niño increased from 2 to 3 yr during the 1960s and 1970s to 4 to 5 yr during the 1980s and 1990s. In addition, before the so-called climate shift that occurred in the late 1970s (e.g., Miller et al. 1994), the development of El Niño started in the east and exhibited westward phase propagation along the equator, while beginning with El Niño in 1982, the development started in the central basin and subsequently exhibited eastward propagation.

The cause and implication of such changes are strongly debated (e.g., Latif et al. 1997); some studies suggest that they can be attributable to global warming, while some are ascribed to internal processes within the climate system. Some specific mechanisms have been identified that can be responsible for changes in the ENSO properties, such as stochastic atmospheric forcing (e.g., Kirtman and Schopf 1998), the influences of extratropical processes in the atmosphere and/or in the ocean (e.g., Gu and Philander 1997; Zhang et al. 1998; Kleeman et al. 1999; Barnett et al. 1999; Schneider et al. 1999), the changes in mean state of the tropical climate system on which El Niño evolves (e.g., Fedorov and Philander 2000; Wang and An 2001), and the nonlinearity and associated parameter changes within a nonlinear climate system (e.g., Münnich et al. 1991; Timmermann and Jin 2002).

Significant interdecadal changes in subsurface temperature structure in the tropical Pacific Ocean were observed in the late 1970s (e.g., Levitus et al. 1994; Zhang et al. 1998) and various potential effects on tropical interannual variability have been suggested. It is well known that on interannual time scales, subsurface thermal variability is a dominant process controlling SST variability in the central and eastern equatorial Pacific where the thermocline is shallow and the mean upwelling is strong. On interdecadal time scales, it has recently been proposed that oceanic teleconnections from the midlatitudes and extratropics can alter the tropical thermal structure and thus could cause variations of El Niño, either by the advection of temperature anomalies through the Pacific subtropical cells (STCs; Gu and Philander 1997) or the changes in the strength of the STCs (Kleeman et al. 1999; McPhaden and Zhang 2002). Here, we use an intermediate coupled

Corresponding author address: Rong-Hua Zhang, ESSIC, University of Maryland, Computer and Space Science Building #224, College Park, MD 20742.
E-mail: rzhang@essic.umd.edu

model (ICM), designed for improved El Niño simulation and prediction in the tropical Pacific Ocean (Zhang et al. 2003), to illustrate the effect of the changes in subsurface temperature structure on ENSO. Some basic questions are investigated. Why are the ENSO properties strikingly different after the late 1970s? Can the changes in the subsurface thermal structure during pre- and postclimate shift periods modulate ENSO properties as observed in the later 1970s? What determines the structure of the coupled modes and the oscillation period within the coupled system?

2. Model descriptions

As illustrated in Fig. 1, we use an ICM consisting of an intermediate dynamic ocean model, a statistical atmospheric model for wind stress ($\boldsymbol{\tau}$), and an SST anomaly model with an empirical parameterization for the temperature of subsurface water entrained into the mixed layer (T_e). The dynamic ocean model was developed by Keenlyside and Kleeman (2002), which is an extension of the McCreary (1981) baroclinic modal model to include varying stratification and partial nonlinearity effects. The atmospheric model is a statistical one constructed from an SVD of the covariance matrix calculated from time series of monthly mean SST and wind stress ($\boldsymbol{\tau}$) fields. Since seasonality in the atmosphere can have an important effect on the onset and evolution of El Niño (e.g., Barnett et al. 1993), we use seasonally varying SVD analyses to construct the $\boldsymbol{\tau}$ model from the period 1963–96. Observed SST data are from Reynolds et al. (2002); wind stress data are the ensemble mean of 24-member ECHAM4.5 simulations, forced by observed SSTAs during the period 1950–99. Using the ensemble mean data allows a better estimate of the signals of atmospheric response to external SST anomalies by smoothing out unrelated atmospheric noise.

An SSTA model is embedded into the dynamic ocean model. The mathematical equation determining the evolution of interannual temperature anomalies in the surface mixed layer can be written as (e.g., Keenlyside 2001; Zebiak and Cane 1987)

$$\frac{\partial T'}{\partial t} = -u'\frac{\partial \overline{T}}{\partial x} - (\overline{u} + u')\frac{\partial T'}{\partial x} - v'\frac{\partial \overline{T}}{\partial y} - (\overline{v} + v')\frac{\partial T'}{\partial y}$$
$$- \{(\overline{w} + w')M(-\overline{w} - w') - \overline{w}M(-\overline{w})\}\frac{(\overline{T_e} - \overline{T})}{H}$$
$$+ \frac{\kappa_h}{H}\nabla_h \cdot (H\nabla_h T') + \frac{2\kappa_v}{H(H + H_2)}(T'_e - T')$$
$$- (\overline{w} + w')M(-\overline{w} - w')\frac{(T'_e - T')}{H} - \alpha_T T'.$$

Here, T' and T'_e are anomalies of SST and the temperature of subsurface water entrained into the mixed layer;

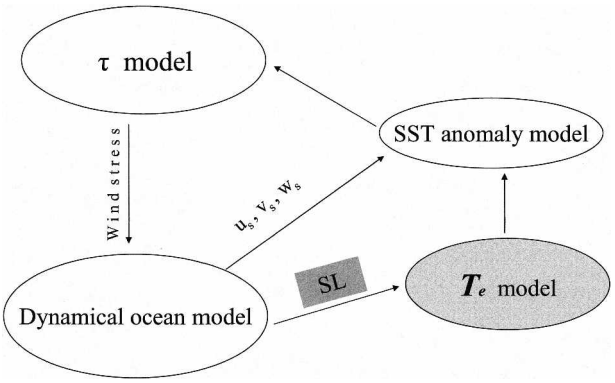

FIG. 1. A schematic illustrating the ICM consisting of a dynamical ocean model, an SST anomaly model, an empirical T_e model, and a statistical atmospheric wind stress (τ) model.

$\overline{T}$ and $\overline{T}_e$ are the prescribed seasonally varying mean SST and T_e from observations; $\overline{u}$ and $\overline{v}$ are the prescribed seasonally varying mean zonal and meridional currents in the mixed layer, and $\overline{w}$ is the prescribed seasonally varying mean entrainment velocity at the base of mixed layer, which are all obtained from the dynamical ocean model; u', v', and w' are the corresponding anomaly fields; H is the depth of the mixed layer; H_2 is a constant (125 m); $M(\delta)$ is the Heaviside step function [i.e., $M(\delta) = \delta$ if δ is positive and $M(\delta) = 0$ if δ is negative]; k_h (2.5×10^3 m^2 s^{-1} meridionally and 2.5×10^4 m^2 s^{-1} zonally), and k_v (10^{-3} m^2 s^{-1}) are the horizontal and vertical diffusion coefficients; $-\alpha_T T'$ is for heat flux which is parameterized as being negatively proportional to the local SSTA with the thermal damping coefficient [$\alpha_T = (100 \text{ day})^{-1}$] estimated from data analyses (e.g., Zebiak and Cane 1987); and other variables are conventional. As expressed, the local rate of SST change (tendency) on the left side is controlled by horizontal advection, entrainment [the $M(\delta)$ terms], anomalous heat flux, horizontal diffusion, and vertical mixing, respectively. Note that T_e is associated with two terms: entrainment across the base of the mixed layer and the vertical mixing between the surface mixed layer and subsurface layer. The function $M(\delta)$ accounts for the fact that SSTAs are affected by vertical advection only when subsurface water is entrained into the mixed layer; but SSTAs can always be influenced by subsurface temperature through vertical mixing.

An empirical T_e model is developed for use in the SSTA model. Making use of the fact that ocean dynamics is the primary source of interannual variability of T_e and SST in the equatorial Pacific, an empirical procedure is proposed to parameterize T_e in terms of sea level (SL) anomalies that are available from the dynamical ocean model (Zhang et al. 2003). Since the SST tendency on the left side can be estimated from observational data, it is possible to determine T_e anomalies by inverting the SSTA equation using observed and

model-produced data. As such, the inverse modeling of T_e, by balancing various terms in the heat budget of the mixed layer, yields an optimized estimate of T_e anomalies for use in simulating SSTAs. A statistical relationship is then constructed from an SVD analysis of the covariance between SL and T_e anomalies to depict their dominant variability patterns. This procedure results in an improved T_e parameterization and allows, relative to other terms contributing to SST variability, a balanced depiction of the thermocline effect on SSTAs by the mean upwelling of anomalous subsurface temperature in SSTA simulations (Zhang et al. 2003).

All coupled model components exchange simulated anomaly fields (Fig. 1). At each time step, the dynamical ocean model produces anomalous sea level, mixed-layer-averaged currents (u_s and v_s), and vertical velocity at the base of the mixed layer (w_s). Then T_e anomalies are parameterized from the SL anomalies. These current and T_e anomalies, together with the prescribed climatology of mean currents from the dynamical ocean model and thermal fields from observations (mean SST and vertical temperature gradient), are passed to the SSTA model to calculate SST anomalies. The resultant SST anomaly is then used to calculate wind stress anomalies with the SVD-based τ model, which force the dynamical ocean model on the next time step. Information between the atmosphere (τ) and the ocean (SST) is exchanged once a day, and the T_e anomalies for the SST model are also updated once a day from the SL anomalies.

3. Numerical experiments

Figure 2 presents anomalies of sea level simulated from the intermediate dynamic ocean model and T_e estimated from the inverse modeling along the equator. The historical SL anomalies are obtained from the ocean model run without the embedded SSTA model, forced by interannual wind stress anomalies from the National Centers for Environmental Prediction–National Center for Atmospheric Research (NCEP–NCAR) reanalysis (Kalnay et al. 1996) for the period 1962–99. The historical T_e anomalies are estimated as follows. First, mean current fields are obtained from the ocean model run forced by climatological NCEP–NCAR winds; current anomalies are taken from the same interannual run producing the SL anomalies. Then, T_e anomalies are estimated from the inverted SST anomaly equation for the period 1962–99 using observed monthly SST fields (Reynolds et al. 2002) and the simulated mean and anomaly currents.

These SL (Fig. 2a) and T_e (Fig. 2b) anomalies are used to construct an empirical relationship between SL and T_e variations via an SVD analysis technique (e.g., Syu et al. 1995), which is performed on all time series data irrespective of seasons. With five SVD modes included, this empirical method can very well reconstruct interannual variability of T_e from a SL anomaly (e.g., Zhang et al. 2005).

To examine the sensitivity of coupled behavior to subsurface temperature variability, three T_e models are constructed separately from three different periods 1963–96, 1963–79, and 1980–96 (T_e^{63-96}, T_e^{63-79}, and T_e^{80-96}, respectively). The cutoffs for the two subperiods for the empirical subsurface temperature (1963–79 and 1980–96) correspond to pre- and postclimate shift that occurred in the late 1970s. Figure 3 shows the spatial patterns of T_e derived from the first pair of singular vectors for the two periods 1963–79 and 1980–96, respectively. Similar to SST variability, that of T_e is concentrated predominantly in the eastern and central basins (largely east of the date line), which represents conditions at the height of El Niño or La Niña events. As with SST, T_e also exhibits interdecadal changes that took place in the late 1970s. As a result, important differences exist in the spatial structure and amplitude of T_e variability during the two periods. For example, during the former period, T_e anomalies are relatively weak both in the eastern equatorial Pacific and in the off-equatorial tropical North Pacific between 140°E and the date line. After the late 1970s, the T_e anomalies are significantly enhanced in the both regions. As such, there are significant differences in the intensity of estimated T_e anomalies from a given SL anomaly using T_e models constructed from these two periods.

The T_e models constructed from each period (T_e^{63-96}, T_e^{63-79}, and T_e^{80-96}) are then utilized to parameterize T_e anomalies from a SL anomaly for use in the SSTA calculations in the coupled system, with other aspects of the model keeping the same (e.g., the τ model used is constructed from the period 1963–96 in all different T_e model runs). Numerical simulations of the coupled system are initiated with an imposed westerly wind anomaly for four months. Evolution of anomalous conditions thereafter is determined solely by coupled interactions within the system. As examined previously by Barnett et al. (1993) and Syu et al. (1995), coupled behaviors can depend on the so-called relative coupling coefficient ($\boldsymbol{\alpha}$), that is, the wind stress anomalies from the τ model may be further multiplied by a scalar parameter before being used to drive the ocean model. To have sustainable interannual variability in the coupled system with different T_e models constructed from differing periods, varying values of $\boldsymbol{\alpha}$ are tested and used in coupled experiments shown below; the dependence of the coupled behaviors on $\boldsymbol{\alpha}$ will be examined later.

4. Results

Incorporating the empirical T_e models into the ICM, the system can simulate self-sustaining ENSO cycles very well with certain values of $\boldsymbol{\alpha}$. For example, the T_e^{63-96} model run with $\boldsymbol{\alpha} = 0.87$ has pronounced inter-

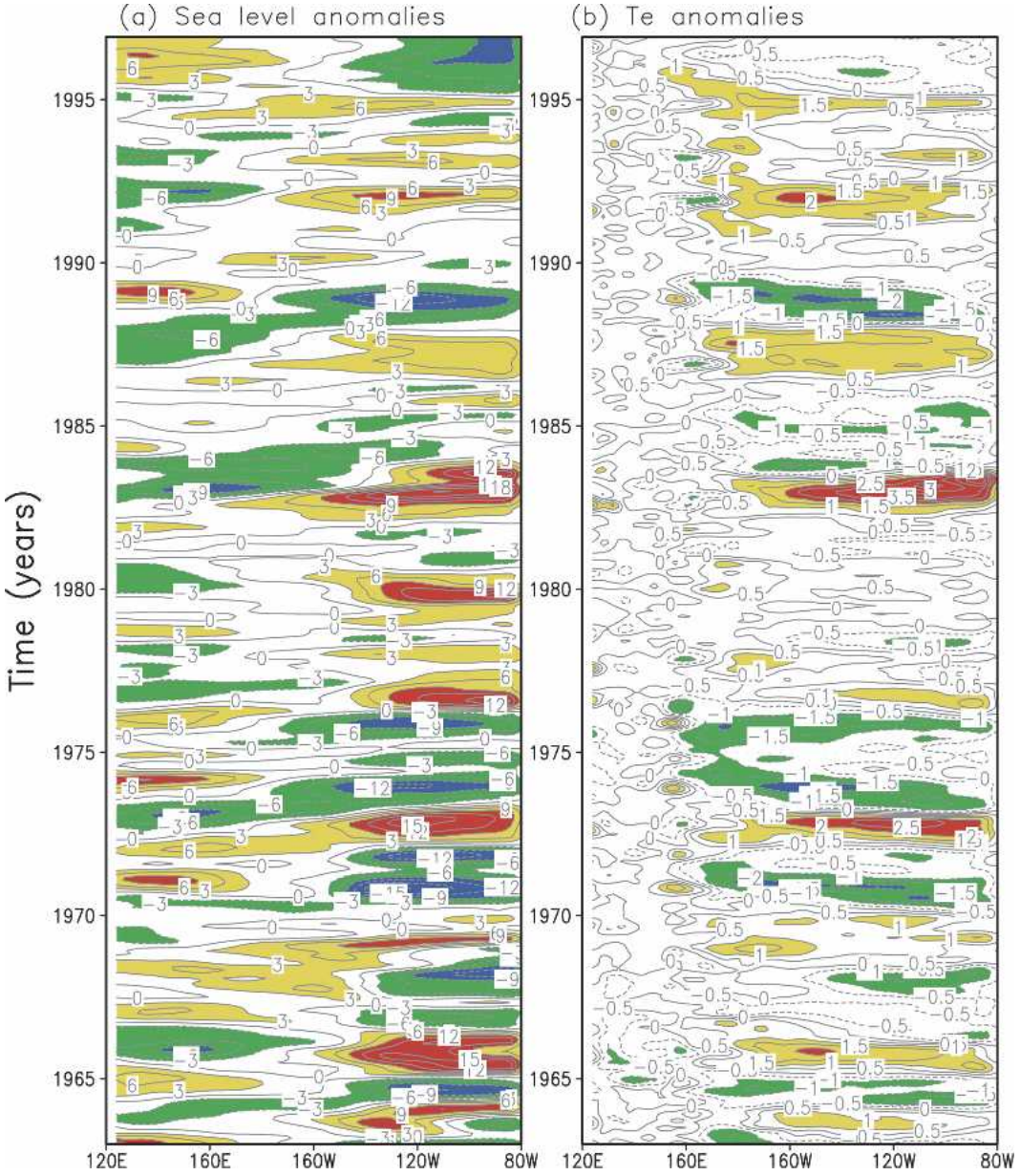

FIG. 2. Anomalies along the equator during the period 1963–96 of sea level (a) simulated from an intermediate dynamic ocean model and (b) T_e estimated from the inverse modeling. The contour interval is 3 cm in (a) and 0.5°C in (b).

annual variability with a major 4-yr period and a dominant standing pattern of SSTAs on the equator (Fig. 4a). To quantify the dominant time scales of variability, spectra are estimated from the Niño-3 SSTAs (Fig. 5a). There are three peaks with enhanced power at different frequencies, the first at 3.6 yr, the second at 5.6 yr, and the third at 2.2 yr, respectively. The first two correspond to the typical El Niño periods of about 3 to 7 yr while the third is at the biennial oscillation period of near 2 yr. The overall time scale of the variability, its structure and the coherent phase relationships among atmosphere–ocean anomalies are consistent with observations.

a. Changes in properties of ENSO

In the T_e^{63-69} model run with $\alpha = 1.35$, the coupled variability is characterized by quasi-biennial oscillations (Fig. 4b). The first enhanced power peak of spectrum estimates (Fig. 5b) is at the biennial oscillation periods (2.2 yr), followed by the second peak at 3.6 yr and the third peak at 2.7 yr, respectively. SST variations are

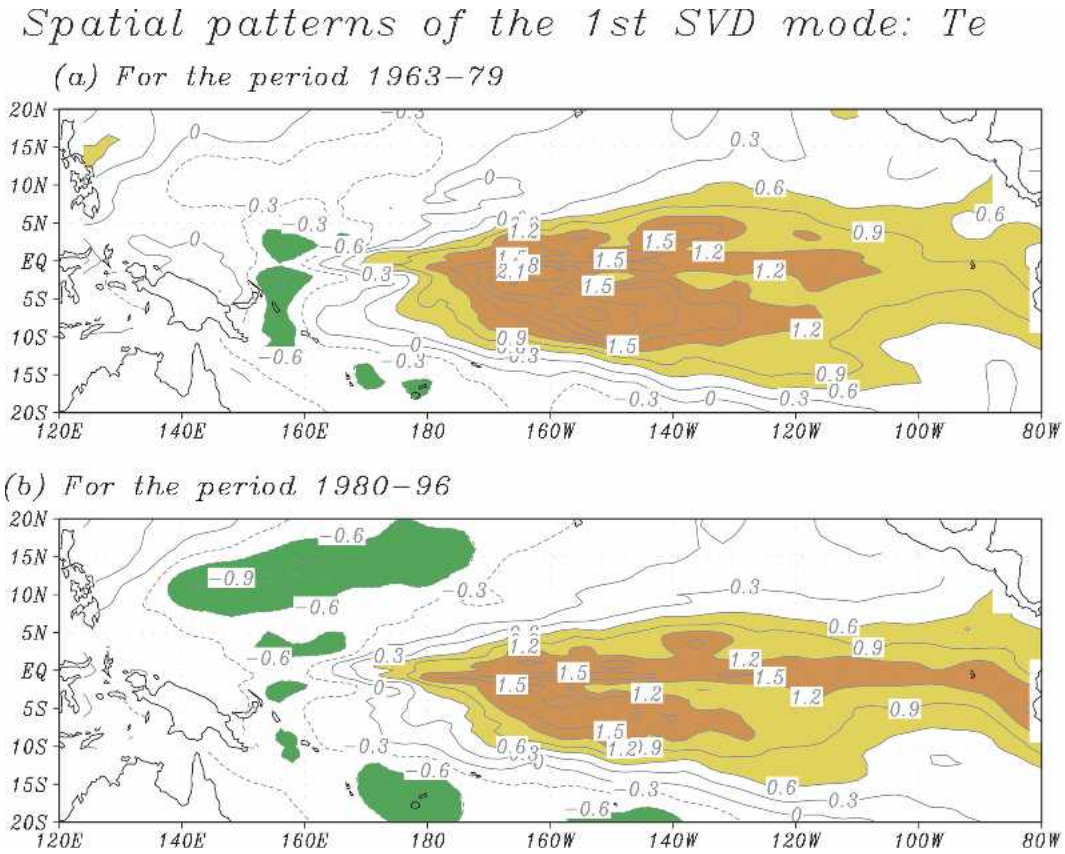

FIG. 3. Spatial patterns of the first leading SVD mode for T_e derived during the periods (a) 1963–79 and (b) 1980–96. The contour interval is 0.3.

predominated by westward propagation along the equator (Fig. 4b), the anomalies first appear in the eastern basin off the coast of South America, thereafter they migrate westward as they amplify with the maximum amplitude near 150°W (Fig. 4b).

Figure 6 further demonstrates the detailed space–time evolution of SST and wind stress anomalies at different periods in the T_e^{63-79} model run. These maps start with El Niño conditions of model year 2 (Figs. 6a,b), proceed to La Niña conditions of year 3 (Figs. 6e,f), and continue to El Niño conditions in year 4 (Fig. 6j). The signal for ENSO transition from one phase (say El Niño) to another (say La Niña) first appears in the eastern equatorial Pacific and along the coastal regions, and then coherent atmospheric and ocean anomalies develop systematically as they propagate westward along the equator. Taking the development of an La Niña event as an example, a cold SST anomaly first emerges in the eastern coastal region (Figs. 6c,d), then it migrates westward along the equator (Figs. 6d–f). As the cold SST anomaly develops, moves further westward, and is present in the central basin, easterly wind anomalies can be seen to develop to the west (Fig. 6e). These anomalies then extend westward into the central and western basin (Figs. 6e,f). Note that the cold SST and easterly wind anomalies grow very rapidly over the eastern–central basin in early year 3 (Fig. 6e), indicating that the atmospheric feedback and local coupled air–sea interactions play a role in amplifying these atmospheric and oceanic anomalies. The following evolution into an El Niño event (Figs. 6h–j) operates in a similar way but with opposite polarity, keeping an interannual cycle going on in the coupled system and a dominant phase propagation from the east to the west along the equator.

In the T_e^{80-96} model run with $\boldsymbol{\alpha} = 0.85$, dramatic changes emerge in the ENSO properties of the coupled system (Fig. 4c), including the time scale and the way El Niño/La Niña events evolve. The coupled system is now characterized by interannual oscillations with a 5 to 6 yr period. The estimated spectra (Fig. 5c) now shift to lower frequency: the first peak at 5.6 yr, the second at 3.6 yr and the third at 2.2 yr. Furthermore, coherent atmospheric and oceanic anomalies originate from the central basin and then propagate eastward along the equator. In contrast to the T_e^{63-79} model run (Fig. 4b), for example, SSTAs first appear in the central basin near the date line, after which they propagate eastward as they amplify, with the maximum amplitude in the eastern basin along the coastal region (Fig. 4c).

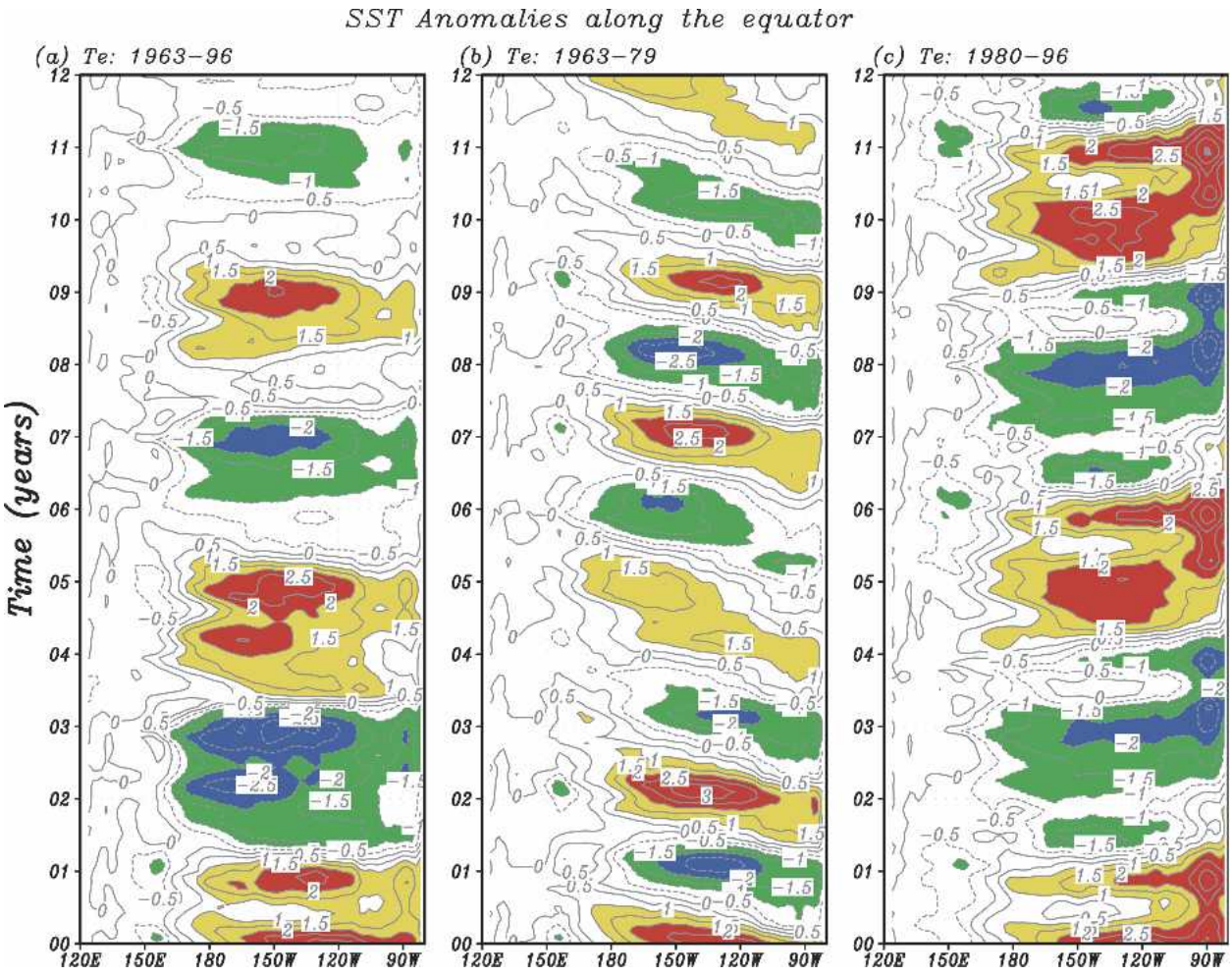

FIG. 4. SST anomalies along the equator simulated in the ICM using the (a) $T_e^{63–96}$, (b) $T_e^{63–79}$, and (c) $T_e^{80–96}$ models. The contour interval is 0.5°C.

The detailed structure of SST and wind stress anomalies simulated from the $T_e^{80–96}$ model run is shown in Fig. 7 for different periods throughout a simulated ENSO cycle. These maps start with the development and decay of La Niña conditions in year 2–3 (Figs. 7a–d), proceed to the initiation, development and decay of an El Niño in year 4–6 (Figs. 7d–i), and continue to the initiation of another La Niña event in early year 6 (Fig. 7i–j). In this case, the ENSO phase starts in the central basin near the date line and then shows eastward propagation along the equator, and finally ends up in the eastern basin. One striking feature during the ENSO cycle is the initial appearance of a pronounced SST anomaly off the equator around 6°–10°N in the central Pacific near the date line. This SST anomaly, accompanied by wind anomalies over the western tropical Pacific, then extends southward into the central equatorial Pacific. Thereafter, the SST and wind anomalies develop systematically and coherently over the central basin, and spread rapidly into the eastern basin, setting up El Niño or La Niña conditions in the east. Taking the development of an El Niño event as an example, a prominent warm SST anomaly, accompanied by westerly wind anomalies, first emerges off the equator at 6°–10°N in early year 4 (Fig. 7d). This SST anomaly then develops and extends southward into the equatorial regions in the central Pacific (Figs. 7e,f). During the development of the El Niño in late year 4 and in year 5, the warm SST and westerly wind anomalies grow rapidly in the central basin (Figs. 7g–i). The westerly wind anomalies depress the thermocline in the east and reinforce the warm SST anomalies there (e.g., Figs. 7h,i), setting up the positive feedback among the wind, thermocline, and SST within the coupled system. So, large SST anomalies are seen to be sustainable in the far eastern equatorial Pacific (e.g., Fig. 7i). At the height of the El Niño event (Fig. 7i), large warm SSTAs (~2°C) cover the whole eastern basin and can persist more than 1 yr (Fig. 4c). At the same time, a cold SST anomaly can be seen to form off the equator at 6°–10°N

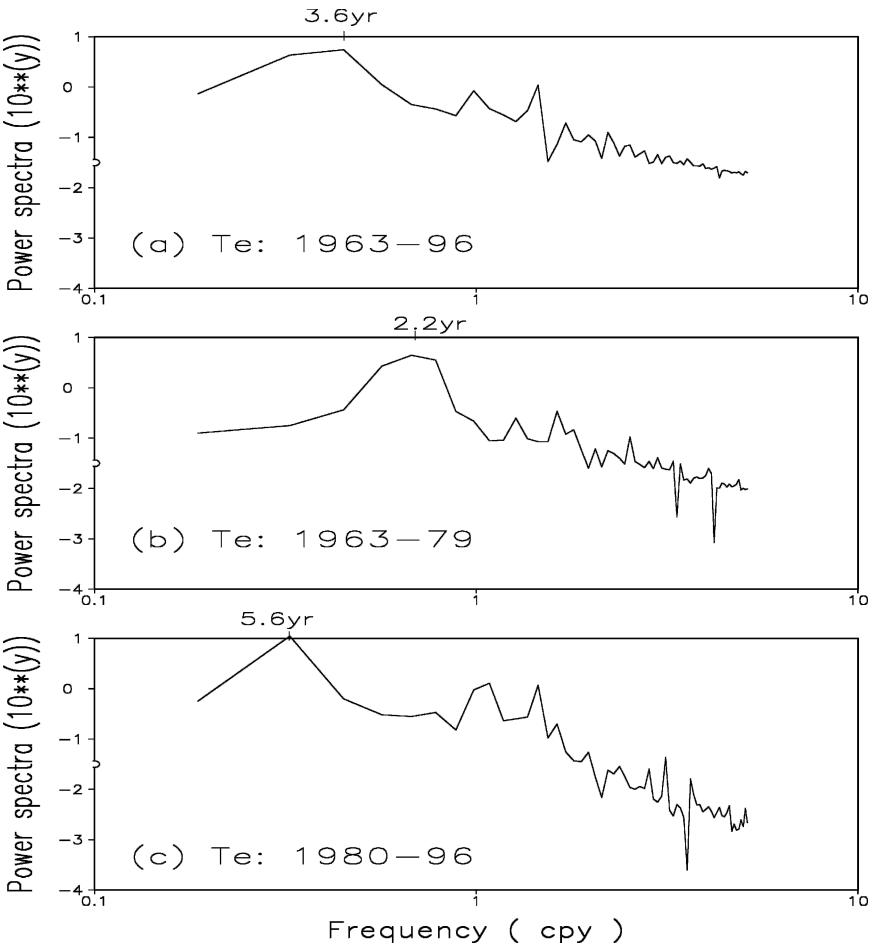

FIG. 5. The spectra of the Niño-3 SST anomalies simulated in the ICM using the (a) T_e^{63-96}, (b) T_e^{63-79}, and (c) T_e^{80-96} models.

near the date line in early year 6 (Fig. 7i), accompanied by easterly wind anomalies in the western Pacific. The subsequent evolution into an La Niña event follows the same route as in the El Niño event but with opposite sense. This pattern of the ENSO onset and development is consistent with the data analyses made by Zhang and Busalacchi (1999) for the 1997–98 ENSO event, suggesting a prominent role of off-equatorial subsurface anomalies along the shallow North Equatorial Countercurrent (NECC) pathway in initiating an SST anomaly off the equator around 6°–10°N near the date line.

b. The possible causes

We analyze the mixed-layer heat budget to identify principal processes causing differences in the simulated SST variability using different T_e models. Figure 8 shows the vertical advection of subsurface temperature anomaly by the upwelling along the equator from the T_e^{63-79} and T_e^{80-96} model runs, respectively. As demonstrated by Jin and An (1999), this term is important for the growth and phase transition of El Niño. In the eastern basin between 160° and 110°W, this term dominates the heat budget while the horizontal advection is important in the western and central parts (not shown). Further east of 110°W, the heat budget is dominated by anomalous horizontal advection (mainly anomalous meridional advection against the mean climatological SST, figures not shown). Thus, through the vertical advection associated with the anomalous T_e, subsurface variability can exert a strong influence on SST variability between 160° and 110°W.

Important differences exist in the vertical advection using the two T_e models. In the T_e^{63-79} case, the vertical advection is characterized by westward propagation along the equator (Fig. 8a), similar to the zonal advection (figures not shown). In addition, the T_e^{63-79} model produces a weak T_e anomaly in the eastern equatorial Pacific (Fig. 3a), resulting in a weak thermocline feedback and allowing the horizontal advection to have a stronger influence on SST variability than the vertical advection. So, using the T_e^{63-79} model, the relative importance of subsurface temperature perturbations ver-

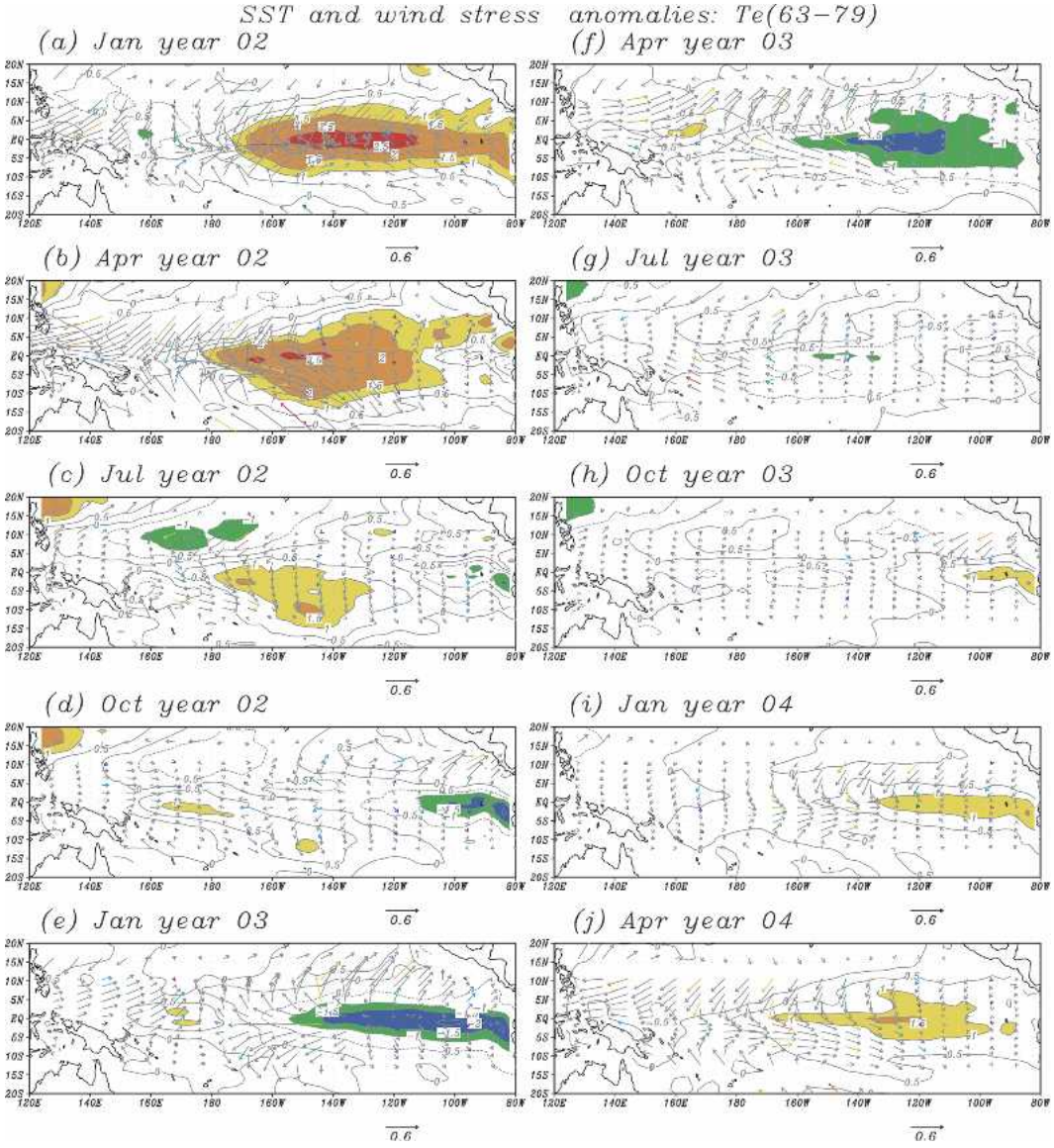

FIG. 6. Horizontal distribution of SST anomalies (contours) and wind stress anomalies (vectors) at different periods simulated from the ICM using the T_e^{63-79} model. The contour interval for SSTAs is 0.5°C and the scale for the wind stress vectors given by the arrow in the low right corner indicates 0.6 dyn cm^{-2}.

sus mixed layer current perturbations in determining SST variability is weakened over the eastern equatorial Pacific, leading to an SST-like mode (e.g., Neelin 1991).

In the T_e^{80-96} model run, the vertical advection term features standing or eastward propagation along the equator (Fig. 8b), which is responsible for the eastward propagation of SSTAs on the equator (Fig. 4c). Since the T_e anomalies produced have larger amplitude both in the central basin off the equator to the north around 6°–10°N and in the eastern equatorial Pacific (Fig. 3b), this term plays a more dominant role in determining SST variability. In the central basin, variations in SL and T_e lead those in SST, which further lead variations in winds, and so coherent oceanic and atmospheric anomalies are seen to originate from the central basin and then propagate eastward along the equator. In the eastern basin, the vertical advection has a larger effect on SSTAs than the horizontal advection, allowing the thermocline feedback to operate more strongly. Once SSTAs are initiated from the central basin and have propagated into the eastern basin, they can grow locally in the east because of the vertical advection through coupled interactions among the thermocline, SST and surface winds, thus sustaining large SSTAs over the eastern basin for more than 1 yr (Fig. 4c).

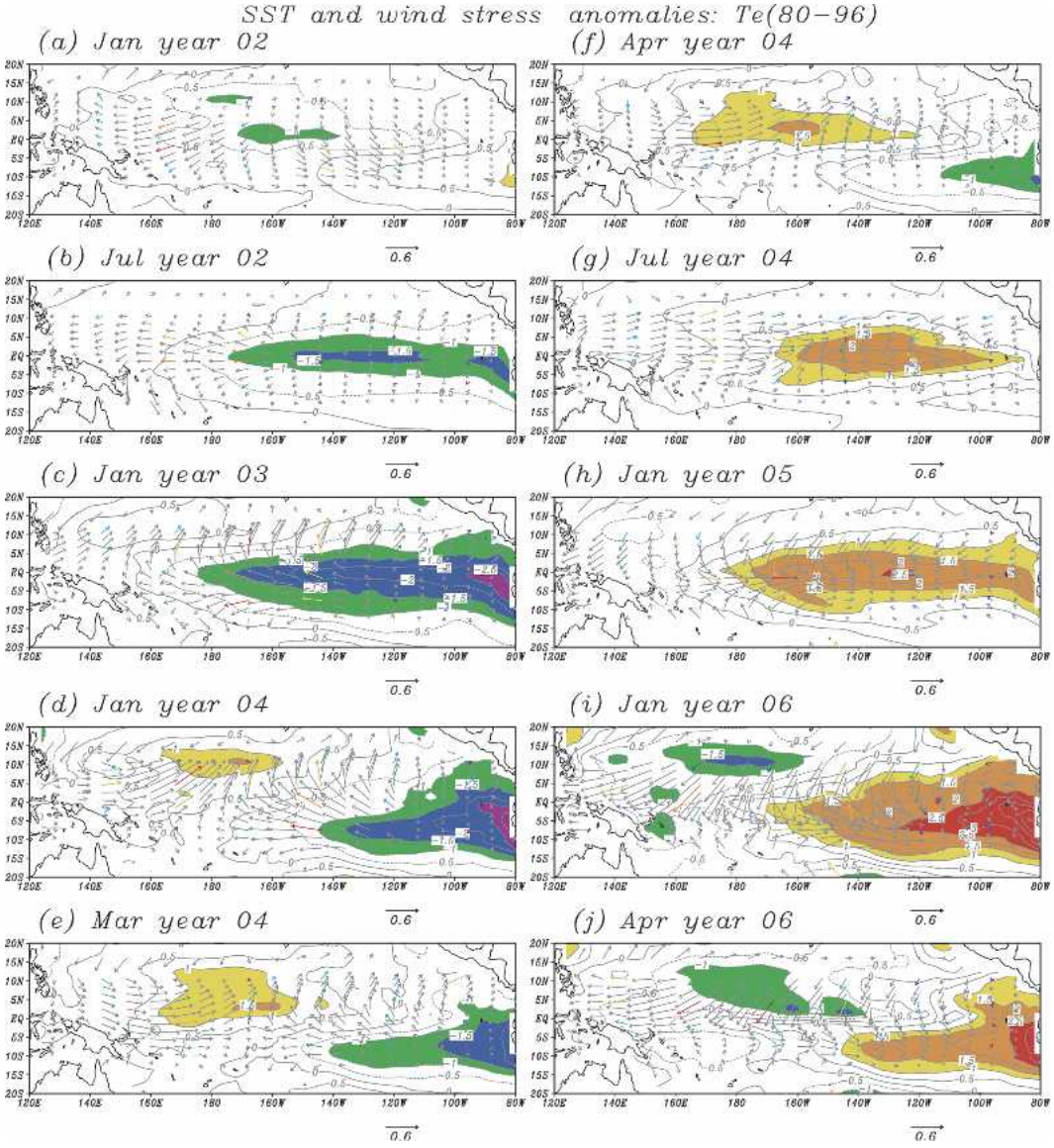

FIG. 7. The same as in Fig. 6 but for the T_e^{80-96} model.

c. The sensitivity to α

It remains to be seen if the changes in the ENSO properties are associated with the coupling strength between the ocean and atmosphere since different $\boldsymbol{\alpha}$ values have been adopted in experiments using different T_e models. A set of further experiments is performed in which $\boldsymbol{\alpha}$ is chosen to be larger or smaller than the standard value ($\alpha = 1.35$ for the T_e^{63-79} model and $\alpha = \mathbf{0.85}$ for the T_e^{80-96} model). Consistent with previous studies (e.g., Syu et al. 1995), the changes of coupling strength can easily modify the amplitudes of the coupled oscillation, but does not have a strong effect on the oscillation periods and the space–time evolution. In general, smaller α (i.e., weak coupling strength between the ocean and atmosphere) results in decreased amplitudes of the coupled anomalies and thus a weak oscillation, but space–time structure is not changed. This is illustrated in Fig. 9 for the T_e^{63-79} model case. Using $\alpha = 1.20$ and $\alpha = 1.00$, the coupled system has a damped oscillation but the periods and space–time evolution features are similar to those with $\alpha = 1.35$ (Figs. 4b and 5b). So, the oscillation period and spatial structure of interannual variability do not seem as sensitive to the changes of the coupling strength as the amplitudes are. Whether or not the coupled system displays a self-sustained oscillation may be not especially important, as the presence of stochastic atmospheric forcing can easily sustain a system that is weakly damped. What are more important are the intrinsic time scales and spatial

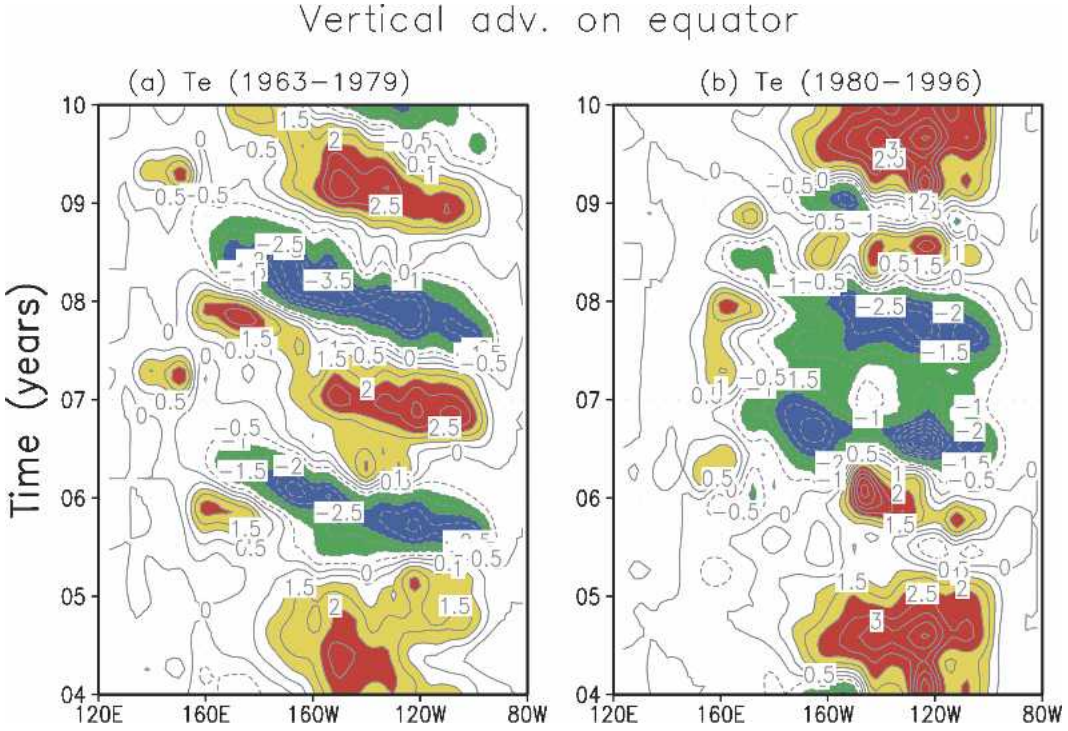

FIG. 8. The vertical advection terms of temperature anomaly by the upwelling $[-(\overline{w} + w')(T'_e - T')/H]$ along the equator from the ICM simulations using the (a) T_e^{63-79} and (b) T_e^{80-96} models. The contour interval is 0.5×10^{-7}°C month^{-1}.

patterns of the deterministic coupled system, which depends sensitively on T_e controlling SST variability.

5. Discussion

An improved ICM is used to examine the effect of interdecadal changes in the structure of subsurface temperature on ENSO properties in the tropical Pacific. Sensitivity experiments are performed using T_e models constructed from the two subperiods (1963–79 and 1980–96), which corresponds to the pre- and postclimate shift observed in the late 1970s. To focus on the role of T_e, no changes are made to other prescribed fields in the ICM [such as the mean ocean fields and the spatial structure of the atmospheric model ($\boldsymbol{\tau}$)]. It turns out that the T_e specification can result in dramatic changes in the simulated interanuual variability, including the oscillation period, structure, and variability characteristics. The manner in which the El Niño- and La Niña-like states evolve and the phase propagation of coherent atmosphere–ocean anomalies are strikingly different using the empirical T_e models constructed from the periods 1963–79 and 1980–96. For example, using the T_e^{63-79} model, the system features a 2-yr oscillation and westward propagation of SSTAs on the equator. Using the T_e^{80-96} model, the coupled system is characterized by a 5 to 6 yr period oscillation and eastward phase propagation on the equator. Heat budget analyses are performed to illustrate that the vertical advection associated with anomalous subsurface temperature is responsible for the change in SST variability and therefore the ENSO properties. Further experiments indicate that although the coupled anomalies become stronger or weaker with different values of the relative coupling coefficient (α), the coupled periods and spatial structure are not significantly changed.

The changes in ENSO properties of the coupled system are consistent with the behavior shift of ENSO that took place in the late 1970s. For example, the simulated interannual SST variability using the two empirical T_e models captures the corresponding observations very well: the ENSO properties simulated using the T_e^{63-79} model correspond to those observed during the 1960s and 1970s, while the T_e^{80-96} model produces the conditions in the 1980s and 1990s. Thus, through numerical experiments, we can answer some basic questions about the interdecadal ENSO variability raised in the introduction. It is demonstrated that the subsurface temperature structure is an important factor controlling the ENSO properties in the tropical Pacific climate system and its changes during the pre- and postclimate shift periods may have modulated ENSO properties as observed in the later 1970s.

Note that the experiments we presented in this work may have biased the role of T_e in modulating ENSO in the coupled model. Since no reliable, basinwide T_e ob-

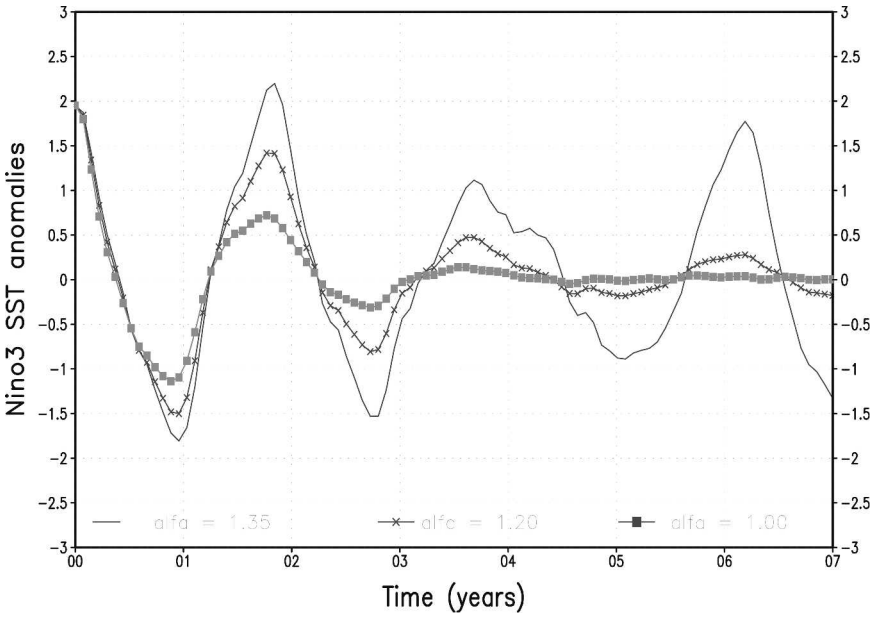

FIG. 9. Monthly time series of the Niño-3 SST anomalies in the ICM runs using the T_e^{63-79} model for different values of α, the so-called relative coefficient.

servations are available at present, an SST anomaly model is used to infer T_e anomalies from observed thermal fields (interannual SST anomalies and mean climatology states of SST and T_e) and simulated currents (interannual anomalies and mean climatology) from an ocean model. This inverse modeling approach is conceived as a means for calculating T_e anomalies in a balanced way, adjusting the various terms of heat budget in the surface mixed layer to produce SST variability as observed. As such, interdecadal changes in SST have been built in the empirical T_e model. Thus, with this procedure, other possible factors affecting interdecadal variability (e.g., changes in winds and the mean ocean states, etc.) can be potentially lumped together in the derived T_e field, possibly biasing the role of T_e in modulating ENSO in the ICM. Another concern involves the estimation of T_e in terms of SL anomalies using an SVD technique. This approach can be justified, since there exists a good relationship between T_e and SL anomalies in the equatorial Pacific on interannual time scales. However, SL anomalies, mainly reflecting a remote dynamic response of the tropical ocean to wind anomalies, may not be the only factor contributing to T_e anomalies, other local thermodynamics can also be important in causing changes in T_e. An empirical parameterization of T_e in terms of SL anomalies from historical data implies that any processes contributing to T_e variability will be included in the model, in so far as these processes are reflected in the SL anomalies. This may also bias the role of T_e in determining interdecadal ENSO characteristics in the coupled system. Further experiments are needed to examine these issues.

This paper has not addressed the origin of the interdecadal changes in T_e, but rather their effects on the ENSO properties. Various processes can cause interdecadal changes in subsurface temperature structure in the equatorial Pacific Ocean, including changes in the strength of STCs and the advection of temperature anomalies through the Pacific STCs. Whatever the causes of interdecadal variability in the Tropics, these changes can be always manifested in the thermocline variability in the equatorial Pacific and hence must impact T_e. Through the empirical T_e models, the interdecadal changes in the subsurface temperature structure that occurred in the late 1970s can be taken into account in our numerical experiments and we are then able to demonstrate its important role in altering ENSO properties in an ICM. We believe that the exact mechanisms of interdecadal variability of ENSO, such as whether it is an intrinsic tropical mode or induced extratropically or whether the oceanic and/or atmospheric bridges connect the subtropics to the Tropics, still remain unresolved. In the near future, we plan to investigate the origin of interdecadal ENSO changes in terms of stochastic atmospheric forcing, nonlinearity, the changes in the mean states of the ocean and/or the atmosphere, and the new factor proposed in this paper, namely, the changes in the subsurface entrainment temperature.

Acknowledgments. We thank R. Murtugudde, S. E. Zebiak, D. DeWitt, N. Keenlyside, R. Kleeman, D. Chen, B. Wang, F.-F. Jin, S. Levitus, and A. V. Fedorov for their comments and suggestions. Zhang is indebted to P. Chang for his help in the SVD-based statistical

analysis. The authors wish to thank anonymous reviewers for their comments. This research is supported by NASA and NOAA.

REFERENCES

An, S.-I., and B. Wang, 2000: Interdecadal change of the structure of the ENSO mode and its impact on the ENSO frequency. *J. Climate,* **13,** 2044–2055.

Barnett, T. P., M. Latif, N. Graham, M. Flugel, S. Pazan, and W. White, 1993: ENSO and ENSO-related predictability. Part I: Prediction of equatorial Pacific sea surface temperature with a hybrid coupled ocean–atmosphere model. *J. Climate,* **6,** 1545–1566.

——, D. W. Pierce, M. Latif, D. Dommenget, and R. Saravanan, 1999: Interdecadal interactions between the tropics and midlatitude in the Pacific basin. *Geophys. Res. Lett.,* **26,** 615–618.

Fedorov, A. V., and S. G. H. Philander, 2000: Is El Niño changing? *Science,* **228,** 1997–2002.

Gu, D.-F., and S. G. H. Philander, 1997: Interdecadal climate fluctuations that depend on exchanges between the tropics and extratropics. *Science,* **275,** 805–807.

Jin, F.-F., and S.-I. An, 1999: Thermocline and zonal advective feedbacks within the equatorial ocean recharge oscillation model for ENSO. *Geophys. Res. Lett.,* **26,** 2989–2992.

Kalnay, E., and Coauthors, 1996: The NCEP/NCAR 40-Year Reanalysis Project. *Bull. Amer. Meteor. Soc.,* **77,** 437–471.

Keenlyside, N., 2001: Improved modeling of zonal currents and SST in the tropical Pacific. Ph.D. thesis, Monash University, 193 pp.

——, and R. Kleeman, 2002: Annual cycle of equatorial zonal currents in the Pacific. *J. Geophys. Res.,* **107,** 3093, doi:10.1029/2000JC000711.

Kirtman, B. P., and P. S. Schopf, 1998: Decadal variability in ENSO predictability and prediction. *J. Climate,* **11,** 2804–2822.

Kleeman, R., J. P. McCreary, and B. A. Klinger, 1999: A mechanism for generating ENSO decadal variability. *Geophys. Res. Lett.,* **26,** 1743–1746.

Latif, M., R. Kleeman, and C. Eckert, 1997: Greenhouse warming, decadal variability, or El Niño? An attempt to understand the anomalous 1990s. *J. Climate,* **10,** 2221–2239.

Levitus, S., T. P. Boyer, and J. Antonov, 1994: *Interannual Variability of Upper Ocean Thermal Structure.* Vol. 5, *World Ocean Atlas 1994*, NOAA Atlas NESDIS 5, 176 pp.

McCreary, J. P., 1981: A linear stratified ocean model of the equatorial undercurrent. *Philos. Trans. Roy. Soc. London,* **298,** 603–635.

McPhaden, M. J., and D. Zhang, 2002: Decadal spin-down of the Pacific Ocean shallow meridional overturning circulation. *Nature,* **415,** 603–608.

Miller, A. J., D. R. Cayan, T. P. Barnett, N. E. Graham, and J. M. Oberhuber, 1994: The 1976–77 climate shift of the Pacific Ocean. *Oceanography,* **7,** 21–26.

Münnich, M., M. A. Cane, and S. E. Zebiak, 1991: A study of self-excited oscillations of the tropical ocean–atmosphere system. Part II: Nonlinear cases. *J. Atmos. Sci.,* **48,** 1238–1248.

Neelin, J. D., 1991: The slow sea surface temperature mode and the fast-wave limit: Analytic theory for tropical interannual oscillations and experiments in a hybrid coupled model. *J. Atmos. Sci.,* **48,** 584–606.

Reynolds, R. W., N. A. Rayner, T. M. Smith, D. C. Stokes, and W. Wang, 2002: An improved in situ and satellite SST analysis for climate. *J. Climate,* **15,** 1609–1625.

Schneider, N., S. Venzke, A. J. Miller, D. W. Pierce, T. P. Barnett, and M. Latif, 1999: Pacific thermocline bridge revisited. *Geophys. Res. Lett.,* **26,** 1329–1332.

Syu, H.-H., J. D. Neelin, and D. Gutzler, 1995: Seasonal and interannual variability in a hybrid coupled GCM. *J. Climate,* **8,** 2121–2143.

Timmermann, A., and F.-F. Jin, 2002: A nonlinear mechanism for decadal El Niño amplitude changes. *Geophys. Res. Lett.,* **29,** 1003, doi:10.1029/2001GL013369.

Trenberth, K. E., and J. W. Hurrel, 1994: Decadal atmosphere–ocean variations in the Pacific. *Climate Dyn.,* **9,** 303–319.

Wang, B., and S.-I. An, 2001: Why the properties of El Niño changed during the late 1970s. *Geophys. Res. Lett.,* **28,** 3709–3712.

Zebiak, S. E., and M. A. Cane, 1987: A model El Niño–Southern Oscillation. *Mon. Wea. Rev.,* **115,** 2262–2278.

Zhang, R.-H., and A. J. Busalacchi, 1999: A possible link between off-equatorial warm anomalies propagating along the NECC path and the onset of the 1997–98 El Niño. *Geophys. Res. Lett.,* **26,** 2873–2876.

——, L. M. Rothstein, and A. J. Busalacchi, 1998: Origin of upper-ocean warming and El Niño change on decadal scale in the tropical Pacific Ocean. *Nature,* **391,** 879–883.

——, S. E. Zebiak, R. Kleeman, and N. Keenlyside, 2003: A new intermediate coupled model for El Niño simulation and prediction. *Geophys. Res. Lett.,* **30,** 2012, doi:10.1029/2003GL018010.

——, R. Kleeman, S. E. Zebiak, N. Keenlyside, and S. Raynaud, 2005: An empirical parameterization of subsurface entrainment temperature for improved SST anomaly simulations in an intermediate ocean model. *J. Climate,* **18,** 350–371.